PCCP

Mechanistic insights into the inhibition of amyloid-β aggregation by chitosan

Journal:	*Physical Chemistry Chemical Physics*
Manuscript ID	CP-ART-01-2023-000162.R1
Article Type:	Paper
Date Submitted by the Author:	08-Mar-2023
Complete List of Authors:	Gotla, Suhas; University of Maryland at College Park, Fischell Department of Bioengineering Matysiak, Silvina; University of Maryland at College Park, Fischell Department of Bioengineering

PCCP

ARTICLE TYPE

Cite this: DOI: 00.0000/xxxxxxxxxx

Mechanistic insights into the inhibition of amyloid-β aggregation by chitosan†

Suhas Gotla,[a] and Silvina Matysiak[a*]

Received Date
Accepted Date

DOI: 00.0000/xxxxxxxxxx

Neurodegeneration related to Alzheimer's disease has long been linked to the accumulation of abnormal aggregates of amyloid-β (Aβ) peptides. Pre-fibrillar oligomeric intermediates of Aβ aggregation are considered the primary drivers of neurotoxicity, however, their targetting remains an unresolved challenge. In response, the effects of macromolecular components of the blood-brain barrier, artificial extracellular matrix mimics, and polymeric drug delivery particles, on the aggregation of Aβ peptides are gaining interest. Multiple experimental studies have demonstrated the potential of one such macromolecule, chitosan (CHT)—a polysaccharide with acid induced cationicity (pKa 6.5)—to inhibit the aggregation of Aβ, and reduce the associated neurotoxic effects. However, the mechanistic details of this inhibitory action, and the structural details of the emergent Aβ complexes are not understood. In this work, we probed how CHT modulated the aggregation of Aβ's central hydrophobic core fragment, $K_{16}LVFFAE_{22}$, using coarse-grained molecular dynamics simulations. CHT was found to bind and sequester Aβ peptides, thus limiting their ultimate aggregation numbers. The intensity of this inhibitory action was enhanced by CHT concentration, as well as CHT's pH-dependent degree of cationicity, corroborating experimental observations. Furthermore, CHT was found to reshape the conformational landscapes of Aβ peptides, enriching collapsed peptides at near-physiological conditions of pH 7.5, and extended peptides at slightly acidic conditions of pH 6.5, where the charge profile of $K_{16}LVFFAE_{22}$ peptides remained unchanged. These conformational changes were limited to peptides in direct contact in CHT, thus emphasizing the influence of local environments on Aβ conformations. These findings add to basic knowledge of the aggregation behaviour of Aβ peptides, and could potentially guide the development of advanced CHT-based materials for the treatment of Alzheimer's disease.

1 Introduction

Neuronal dysfunction in Alzheimer's disease (AD) is closely associated with the abnormal accumulation of proteinaceous aggregates in the brain. The accumulation of amyloid-β (Aβ) peptides in particular has emerged as a key event in early AD. In the decades leading up to the appearance of cognitive symptoms in AD patients, Aβ undergoes progressive accumulation into pre-fibrillar oligomers (PFOs), and eventually to fibrillar plaques in the interneuronal spaces of the central nervous system.[1–3] Interestingly, a growing body of evidence implicates PFOs—not fibrils—in neuronal dysfunction and degeneration, challenging the long-held belief that plaques were the primary neurotoxic agents in AD.[4,5]

Unfortunately, drug candidates targetting neurotoxic PFOs are seeing muted success in clinical trials.[6] Limited bioavailability across the blood-brain barrier (BBB) and poor specificity for the transient and heterogeneous structures of PFOs have come to light as major bottlenecks for anti-AD drug development.[6–9] In an effort to address these pitfalls, macromolecular components making up extracellular matrices (ECMs), the BBB, and drug carrying vehicles, have garnered a renewed interest as potential influencers of Aβ aggregation.

Polysaccharides are one such class of macromolecular components that are known to have drastic effects on the outcomes of Aβ aggregation.[10–13] In particular, the chitin-derived chitosan (CHT) polysaccharide is a common ingredient in ECM-mimetic scaffolds[14,15] and BBB-permeable drug carriers[16–18] that inhibits Aβ aggregation. Thioflavin T (ThT) fluorescence, circular dichroism, and atomic force microscopy experiments have revealed that the co-aggregation of Aβ with increasing concentrations of CHT yields smaller, and more disordered aggregates with reduced beta-sheet contents.[10–12] Notably, CHT's N-glucosamine saccha-

[a] *Fischell Department of Bioengineering, University of Maryland, College Park, MD, USA. E-mail: matysiak@umd.edu*

[*] *Corresponding author*

† Electronic Supplementary Information (ESI) available: Supporting figures for CHT's effect on Aβ aggregation kinetics, and peptide conformations; Supporting tables of forcefield parameters. See DOI: 10.1039/cXCP00000x/

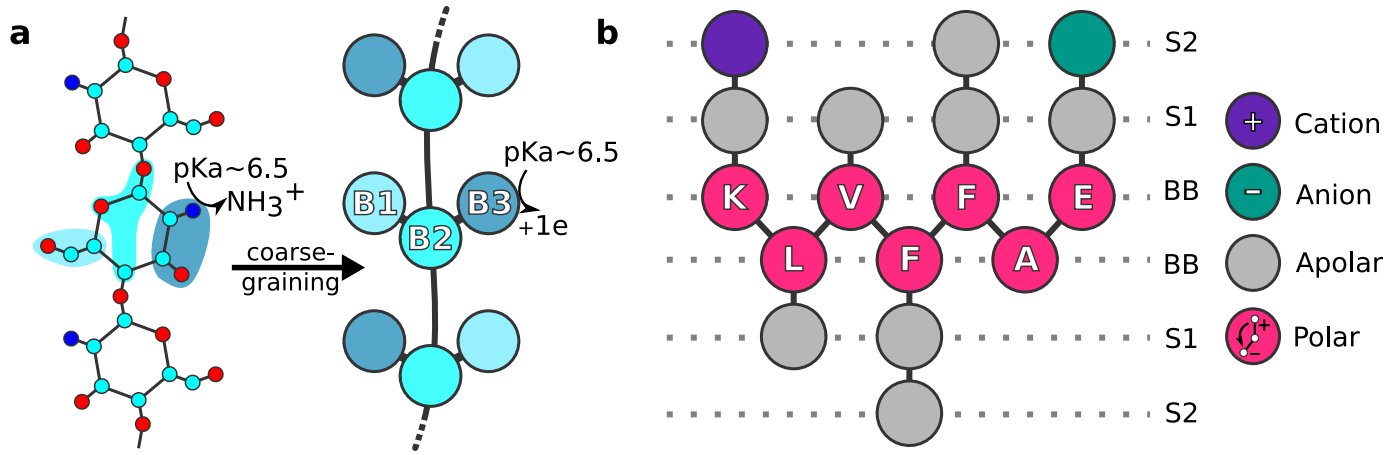

Fig. 1 (a) CG model for CHT along with its corresponding atomistic structure. (Left) In the atomistic structure, cyan, blue, and red spheres represent carbon, nitrogen, and oxygen atoms, respectively. (Right) The CG beads, B1, B2, and B3 are all polar, and coloured in the order of increasing polarity B1<B2<B3. The ionizable bead B3 has a pKa of 6.5. (b) CG model for the K_{16}LVFFAE$_{22}$ fragment of the Aβ peptide. BB beads represent the peptide backbone, and S1 and S2 represent amino acid side chain beads. Beads are coloured according to the legend on the extreme right.

ride units contain an ionizable amine with a pKa close to 6.5 that renders CHT slightly cationic at neutral pH, highly cationic at strongly acidic pH, and electrostatically neutral at basic pH. Accordingly, Liu *et al.* have found that the intensity of CHT's inhibition of Aβ aggregation is also enhanced by CHT's degree of cationicity.[11]

Although the smaller sizes, and reduced beta-sheet contents of the products of Aβ-CHT co-aggregation are consistent with the properties of toxic Aβ PFOs, mortality studies in cells and animal models have found that CHT neutralizes Aβ-mediated cytotoxicity.[13,16,19,20] These paradoxical results indicate that the toxicity of Aβ aggregates is not solely determined by their size and degree of secondary structure organization. In this work, we aim to understand the mechanistic and nanoscale details of CHT's influence on Aβ-aggregation with the broader goal of understanding the origins of CHT's neuroprotective properties against Aβ-mediated pathology.

Biophysical techniques like ThT fluorescence and CD can indirectly measure secondary structure content in Aβ aggregates as a function of time, but cannot generate nanoscale structural details. On the other hand, AFM can generate detailed nanoscale snapshots of Aβ aggregates, but time-resolved data collection can be very challenging. While computational molecular modelling techniques can somewhat bridge the divide between structural detail and temporal dynamics, free energy barriers can prove to be computationally prohibitive to overcome with conventional methods for large supramolecular processes such as the aggregation of Aβ with CHT. Understandably, past computational modelling efforts have been limited in scope, focussing on docking and short atomistic molecular dynamics (MD) simulations of single CHT chains on preformed Aβ protofibrils.[10,11] Here, we opt for the coarse-grained (CG)–MD approach, whereby the topological representations of molecules are simplified by grouping chemically similar atoms into CG beads. Relative to atomistic MD, CG–MD compromises some accuracy and precision in favour of wider sampling of the free energy landscape, thus allowing for a balance between long timescales and large length-scales conducive to a competent exploration of the mechanistic underpinnings of the interactions between CHT and Aβ.

Thus, co-assembly of Aβ and CHT was performed across a range of Aβ:CHT molar ratios, and two pH conditions using CG-MD. Aβ was modelled using a minimalistic model fragment K_{16}LVFFAE$_{22}$, which encompasses the amyloidogenic hydrophobic core of Aβ, as well as the acidic E$_{22}$ residue that was determined to be a major site for interaction with CHT in previous docking studies.[11] CHT was modelled as a fully deacetylated sequence of N-glucosamine saccharide units with pH-dependent degrees of cationicity. Based on the popular explicit solvent MARTINI forcefield,[21] the CG models used in this work for CHT and Aβ have been extensively validated in previous studies.[22–25] We discuss how CHT, at varying cationicities and concentrations, affects the kinetics of Aβ aggregation and the conformational fates of the constituent peptides. The mechanistic insights presented in this paper add to basic knowledge of the interactions of Aβ with CHT that may assist the improvement and development of biomedical products for AD therapy. We discuss the results of our simulations and develop a mechanistic picture of CHT's inhibitory effect on Aβ aggregation.

2 Methods

CG model details. The CG models for CHT and Aβ used in this work have their roots in the popular MARTINI forcefield for biomolecules.[21,26] CHT is modelled as 100% deacetylated, chains of N-glucosamine saccharide units. Each N-glucosamine saccharide is represented by three CG-beads: B1, B2, and B3 (Fig. 1a), each of which map to three-to-four fine-grained heavy atoms. To account for N-glucosamine's ionizable 2'-amine group, a charge of +1e is applied to a fraction of B3 beads, as determined by the desired environment pH and the Hendersen-Hasselbalch relation. Previous publications provide further details of this model, and demonstrate its ability to reproduce CHT's helicity, pH-dependent gelation, and mechanical properties.[22,23]

The K_{16}LVFFAE$_{22}$ peptide fragment was modelled with the group's WEPPROM forcefield, where each residue is represented by one backbone (BB) bead, and up to three sidechain beads.[27] While most of the bead definitions and interaction levels in WEPPROM are identical to those of MARTINI, there are two salient differences between them. First, protein backbones in WEPPROM are modelled with polarized beads (BB bead in Fig. 1b) that have internal Drude-like oscillating charges to emulate the inherent dipole moments of peptide bonds.[27] Van der Waals interactions of these polarized beads, with other polarized and charged beads, were scaled down to compensate for the added electrostatic interactions through the internal dummy charges. Second, the interactions of the hydrophobic sidechains of L17 and V18, and solvent particles were significantly reduced to enable the folding of beta-sheets.[28] Details on the bonded and nonbonded interaction parameters of the WEPPROM Aβ peptide model can be found in Sahoo *et al.* (2019).[24] All other nonbonded interactions, including those between CHT and K_{16}LVFFAE$_{22}$, are identical to MARTINI levels.[26] See Table S1 for the bead types associated with every residue of CHT and Aβ K_{16}LVFFAE$_{22}$, and Table S2 for the Lennard-Jones interaction parameters between all the bead types used in this work.

The MARTINI polarizable water model[29] was used as the solvent in our simulations. Standard MARTINI monovalent ions were used to balance net-charge where necessary.

Simulation details. Aβ concentration was fixed at roughly 36 mM while CHT concentrations spanned 0, 0.3, 1.5, and 3% (w/v). The effective molar ratios of Aβ to N-glucosamine saccharide units of CHT were within the range of Liu *et al.*'s experimental studies.[11] The 0% CHT system containing only Aβ peptides and solvent serves as a control system. Cationic charge was assigned randomly across CHT's N-glucosamine saccharides in proportion with the pH conditions (as determined by the Hendersen-Hasselbalch relation): 10% at pH 7.5, and 50% at pH 6.5. The K_{16}LVFFAE$_{22}$ Aβ sequence remains isoelectric in this pH range, and thus the 0% CHT control system does not change with pH.

The initial configurations were set up as follows. In a $18 \times 18 \times 18$ nm cubic periodic box, 100 molecules of unstructured Aβ peptides (36 mM), and 0, 2, 10, or 20 CHT chains (for 0, 0.3, 1.5, and 3.0% w/v, respectively) were inserted at random positions. Each box was solvated with about 41,000 MARTINI polarizable solvent particles, and excess charge was neutralized with counterions. The initial structures were equilibrated with 10,000 steps of steepest descent energy minimization, followed by 5000 steps of NPT simulation at 0.01 ps timesteps with position restrained solute molecules. Finally, 700 ns of unrestrained NPT MD was performed with timesteps of 0.01 ps. We used the leapfrog integrator in conjunction with the Nose-Hoover thermostat at 300 K with a time constant of 1 ps.[30] Pressure was maintained at 1 bar with an isotropic Parrinello-Rahman barostat, with 5 ps time constants, and compressibility of 3.5e-5 bar^{-1}.[31] Short range Van der Waals interactions were smoothly scaled to zero between 0.9 to 1.2 nm, while short range electrostatics were calculated with a plain cutoff of 1.6 nm. Long range electrostatics were computed with the Particle Mesh Ewald scheme with relative electrostatic permittivity of 2.5.[32] LINCS was used to constrain the dummy bonds within the MARTINI polarizable solvent particles.[33] All simulations were performed using GROMACS 2019.[34] Two independent replicas with unique initial velocities were performed for each CHT concentration-pH pair.

Evaluation of Aβ peptide and aggregate properties. An Aβ aggregate is defined by two or more peptides with at least one inter-peptide BB-BB contact (0.7 nm cutoff). To qualify as a beta-sheet, at least 4 out of 7 possible pairs of internal backbone dipoles had to be aligned between peptides. An aggregate can have a heterogeneous composition of smaller constituent beta-sheets.

To qualify as an alpha-helix, the backbone dipoles of at least two out of three possible $i \rightarrow i+4$ residue pairs, K_{16}-F_{20}, L_{17}-A_{21}, and V_{18}-E_{22}, had to be aligned.

End-to-end distance (r_{e2e}) of an Aβ peptide is measured between the BB beads of K_{16}, and E_{22}. For a peptide to be considered associated with CHT, at least one BB bead had to be in contact with any of the beads on a CHT molecule (0.7 nm cutoff).

In this manuscript, the term "peptide" refers to any molecule of Aβ at any state, whereas the term "monomer" specifically refers to un-aggregated Aβ peptides with aggregation number, $N = 1$. By extension, the term "multimer" refers to an aggregated cluster of Aβ peptides with aggregation number, $N > 1$.

3 Results and Discussion

3.1 CHT inhibits Aβ aggregation by peptide sequestration and promotion of small multimers

At 0% CHT, Aβ aggregation occurred in two phases: an initial growth phase from 0 to 300 ns, followed by a stationary phase from 300 to 700 ns. The populations of monomers, and the sizes of the largest multimers were tracked. During the growth phase, a rapid loss of monomers was observed (maroon trace in Fig. 2a, 0-50 ns), while multimers steadily grew and coalesced until nearly all peptides had incorporated into a single large aggregate (maroon trace in Fig. 2c, 0-300 ns). During the stationary phase, the size of the largest multimer remained constant, indicating that the aggregation process had reached quasi-equilibrium (maroon trace in Fig. 2c, 300-700 ns).

The addition of CHT influenced both phases of Aβ aggregation in a concentration dependent manner. First, dampening was observed in the rate of monomer decay: while Aβ monomers disappeared well within 50 ns in the 0 % CHT (w/v) control case, monomer decay continued at least until 300 ns at 0.3 % CHT (w/v). Similarly, monomers continued to decay until about 300 ns at 1.5 and 3.0% CHT (w/v), but residual populations of around 40 and 60 peptides, respectively, remained as monomers throughout the stationary phase.

Tracking the CHT-associated subpopulation of Aβ monomers (Fig. 2b) helped us understand the mechanics behind this dampening effect. Between 0 and 30 ns, Aβ monomers rapidly absorbed onto CHT chains, peaking at roughly 4, 15, and 25 monomers at 0.3, 1.5, and 3.0 % CHT (w/v), respectively. Following the peak, a gradual decay of CHT-associated monomers was observed until a plateau was reached.

The decay of CHT-associated monomers could potentially be

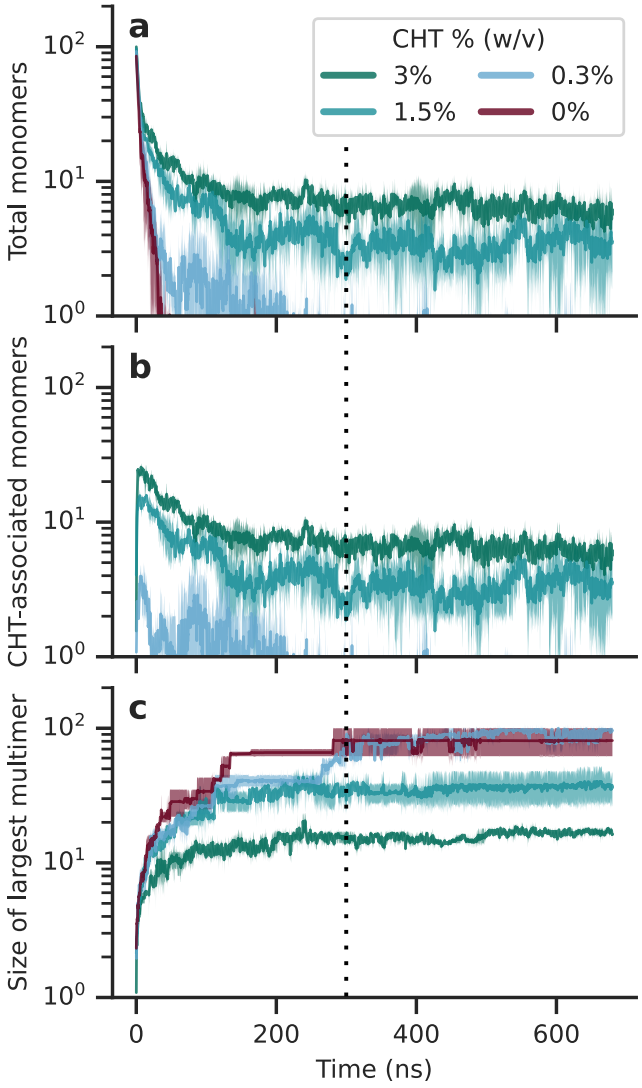

Fig. 2 Time evolution of Aβ aggregation at pH 7.5, with 0, 0.3, 1.5, and 3.0 % CHT measured by total population of monomers (a), CHT-associated subpopulation of monomers (b), and size of the largest multimers (c). The vertical line at t=300 ns demarcates the growth phase (t $<$ 300 ns) from the stationary phase (t $>$ 300 ns). Time series are averaged over two independent runs, and the shaded regions denote standard deviation.

explained by the following reasons:

1. Unbinding of peptides from CHT's surface.
2. Aggregation of CHT-associated monomers with other peptides, leading to loss of their monomer status.

Populations of free monomers, i.e., non-CHT-associated monomers, disappeared long before the CHT-associated monomer decay plateaued (Fig S3 a-c), thus implying that CHT-Aβ complexes were stable and unlikely to break. As a result, the possibility of CHT-peptide unbinding contributing to the observed decay was ruled out. Consequently, only aggregation of CHT-associated monomers could explain the decay in their populations. Two mechanisms of CHT-associated monomer aggregation were observed: (1) deposition of bulk peptides onto CHT-associated monomers, and (2) the diffusion of peptides along CHT fibres and the consequent aggregation of CHT-associated Aβ peptides with each other. While both mechanisms were likely in the initial stages of aggregation, the second mechanism dominated the later stages where all bulk monomers (Fig. S3), and all bulk multimers (Fig. S4) had been depleted.

Plateauing of CHT-associated monomer populations revealed that not all CHT-associated monomers were able to aggregate (see traces for 1.5% and 3% CHT in Fig. 2a, and b). These residual populations of CHT-associated monomers were indicative of sequestration of peptides, monomeric or otherwise, by CHT. Both peak, and residual populations of CHT-associated monomers increased with CHT concentration, implying that the sequestering effect of Aβ peptides by CHT was concentration dependent. An associated outcome was the reduction in the overall size of multimers, in terms of aggregation number: while the largest multimers reached maximum sizes of around 100 peptides at 0 and 0.3% CHT, they were capped at approximately 30 and 15 peptides at 1.5 and 3.0 % CHT, respectively (Fig. 2c).

The reduction in multimer size was also visually apparent during the final $\sim$ 100 ns of the quasi-equilibrium phase, across the different self-assembly conditions. Fig. 3 shows representative snapshots of these quasi-equilibrium conformations: a large 100-mer Aβ aggregate can be observed at the 0% CHT control system (Fig. 3a), and progressively smaller and more numerous multimers can be observed at 0.3, 1.5, and 3.0 % CHT (Fig. 3b, c and d).

In a nutshell, by absorbing Aβ peptides, CHT acted as a sink for monomers and other low-aggregation number states. While some CHT-associated monomers could aggregate with each other and peptides from the bulk, many remained sequestered. Furthermore, as CHT concentrations increased, more peptides were sequestered, and the inhibition of Aβ multimer growth became stronger. These results are in good agreement with ThT fluorescence measurements from past studies showing a decrease in Aβ fibrillation with increasing concentrations of CHT.[11]

3.2 CHT's degree of cationicity strengthens inhibitory mechanisms

Liu *et al.* also found that modified CHT molecules with significantly higher charge had a much stronger inhibitory effect on Aβ fibrillation.[11] To explore the influence of CHT's degree of cationicity, we performed additional co-assembly simulations with the same Aβ:CHT molar ratios at pH 6.5, where the isoelectric nature of Aβ was preserved but CHT chains were much more cationic, with 50% of their monomers being charged.

CHT concentration dependent phenomena of monomer decay dampening, increase in residual monomer populations, and reduction in the size of the largest multimers were also observed at pH 6.5, albeit in a stronger fashion relative to the same concentrations at pH 7.5. Comparison of Fig. 2b and Fig. S1 (b) illustrates why this is. The peak populations of CHT-associated monomers are roughly the same for each CHT concentration at pH 6.5 and pH 7.5. As with pH 7.5, free monomer populations also disappear well before CHT-associated monomer decays plateau at pH 6.5

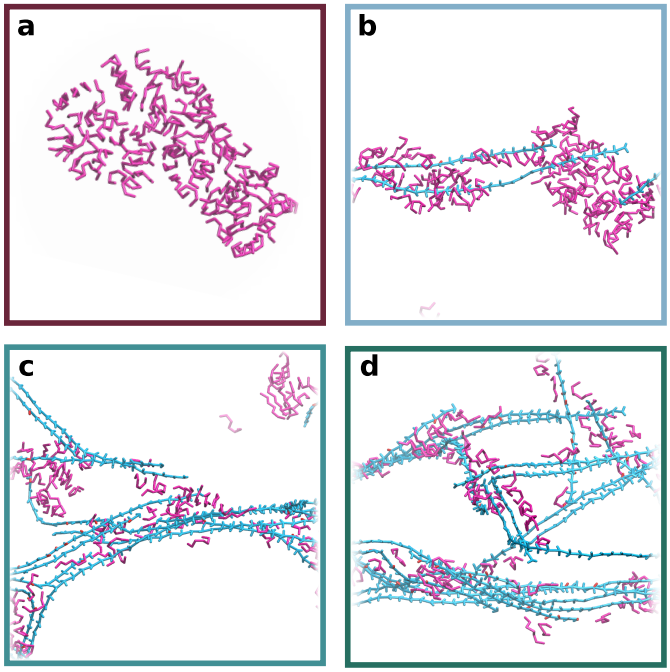

Fig. 3 Snapshots representative of quasi-equilibrium conformations of Aβ self-assembly with 0% (a), 0.3% (b), 1.5% (c), and 3% (d) CHT (w/v) at pH 7.5. Backbones (BB beads) of Aβ peptides are represented in magenta. CHT molecules are represented as cyan chains, except for protonated B3 beads, which are coloured red. Solvent particles, dummy charges of BB beads, and S1 and S2 side chain beads are hidden for clarity.

(Fig. S3 d-f). But, the decay of CHT-associated monomers is significantly muted at pH 6.5. In the case of 3% CHT at pH 6.5, the decay of the peak population is almost imperceptible. Ultimately, by the end of the self-assembly simulations at pH 6.5, residual populations of roughly 25, 10 and 1 CHT-associated monomers remain at 3.0, 1.5, and 0.3% CHT, respectively. On the other hand, residual populations of about 7, 5 and 0 peptides remain at the end of self-assembly for 3.0, 1.5, and 0.3% CHT at pH 7.5 respectively. These results indicate that the sequestration of monomeric peptides by CHT is significantly stronger at pH 6.5 compared to pH 7.5. This strengthening effect is attributed to the enrichment of electrostatic interactions between Aβ and the greater numbers of cationic N-glucosamine units in CHT chains at pH 6.5.

We also observed a shift in the extent of Aβ aggregation from distributions of weighted aggregation numbers (Fig. 4a). Each N-mer is represented N times in the data, such that we have equal numbers of data points across the different conditions. For each pH-CHT concentration pair, the distributions were constructed from the last 50 ns across the two independent replicas. At each CHT concentration, Aβ aggregation numbers trended lower at pH 6.5, compared to pH 7.5. This observation of increased inhibitory activity of CHT at pH 6.5 corroborates previous experiments, where increasing CHT's cationicity was shown to enhance the inhibition of Aβ fibrillation within Aβ's isoelectric pH range. [11]

In summary, CHT's concentration-dependent mechanism of Aβ aggregation inhibition by binding and sequestering Aβ peptides from bulk solution, is strengthened by increasing its degree of cationicity, and is conserved at pH 6.5-7.5.

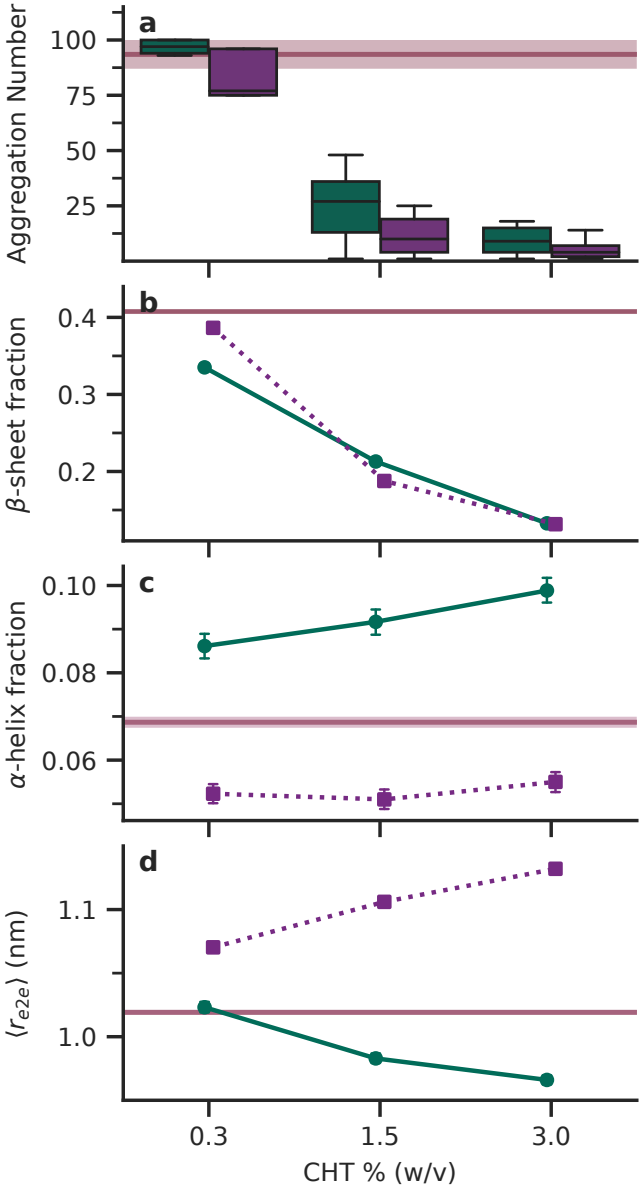

Fig. 4 Distributions of weighted aggregation numbers of Aβ peptides (a), beta-sheet fractions in Aβ aggregates (b), alpha-helix fraction in Aβ aggregates (c), and mean end-to-end distance ($\langle r_{e2e} \rangle$) of Aβ peptides (c) in self-assembled systems. Data for the 0% CHT control case are shown in shaded maroon regions, while data for Aβ-CHT self-assemblies at 0.3-3.0 % CHT at pH 7.5 and pH 6.5 are shown in green (specifically, green circles joined by solid lines in (b)-(c)) and purple (specifically, purple squares joined by dotted lines in (b)-(c)), respectively. Data are taken from the last 50 ns of the self-assembly simulations, and error bars in (b)-(d) indicate standard errors of mean.

3.3 CHT's impact on the conformational properties of Aβ peptides

In addition to suppression Aβ's ability to form fibrils, circular dichroism measurements show that CHT also significantly suppresses Aβ's ability to form beta-sheet secondary structures. [10,19]

This section explores how conformational properties of Aβ peptides are impacted by CHT concentration and cationicity.

At 0% CHT, roughly two-fifths of all the peptides participated in beta-sheets (maroon shaded region in Fig. 4a). With added CHT, prevalence of beta-sheets in our self-assemblies decreased with increasing CHT concentrations at pH 7.5 (green trace in Fig. 4b), as well as pH 6.5 (purple trace in Fig. 4b). The influence of CHT's pH-dependent degree of cationicity on beta-sheet secondary structure fractions ranged from minimal (Fig. 4b at 0.3% CHT) to insignificant (Fig. 4b at 1.5%, and 3.0% CHT).

On the other hand, populations of alpha-helical structures displayed stronger dependences with concentrations and cationicities of CHT (Fig. 4c). At pH 7.5, helical populations were significantly enriched in a concentration dependent manner: at 0.3% CHT, helical populations reached about 9%, and incrementally increased to about 10% at 3% CHT. Although subtle, the upward trend is statistically significant considering the standard errors of mean. In contrast, helical populations plummeted at pH 6.5, and hovered between 5.5% and 6% in the presence of CHT. Thus, CHT acts as an inducer of helical conformations at pH 7.5, and as a repressor of helical conformations at pH 6.5.

Analysis of mean end-to-end distances ($\langle r_{e2e} \rangle$) between the BB beads of K_{16} and E_{22} of Aβ peptides at these different conditions offer some explanations to these results. While $\langle r_{e2e} \rangle$ decreased at pH 7.5 with CHT concentration (green trace in Fig. 4d), the opposite was observed at pH 6.5 (purple trace in Fig. 4d), where end-to-end distances increased with CHT concentration.

Collapsed peptide geometries are conducive to the formation of alpha-helices, while extended conformations are not. The stabilization of collapsed conformations by CHT at pH 7.5 explains why helices are enriched compared to 0% CHT. On the other hand, the stabilization of extended conformations by CHT at pH 6.5 explains why helices are depleted compared to 0% CHT.

Extended peptide geometries also decrease the energy barriers for beta-sheet formation by maximizing the availabilities of peptide backbones for inter-peptide interactions. Therefore, although the lower aggregation numbers at pH 6.5 are disadvantageous for the formation of beta-sheet rich aggregates, the disadvantage is counter-balanced by the reduced energy barriers for beta-sheet formation afforded by the relatively extended peptides. The outcome of these competing forces is that the beta-sheet fractions at pH 6.5 and 7.5 are roughly the same. (Fig. 4b).

In summary, the conformational properties of Aβ peptides are a product of complex and sometimes competing actions of CHT concentration and cationicity. The CHT concentration-dependent decrease in beta-sheet secondary structure is in agreement with previous experimental studies.[10,11,16,19] Helical conformations in Aβ have been previously reported by Jha *et al.*[12] in their studies with CHT-based anti-amyloid nanoparticles. Our results indicate that the concentrations of helical Aβ conformers is contingent on CHT concentration and degree of cationicity.

3.4 Aβ conformational change requires direct contact with CHT

This section aims to provide a deeper understanding of the direct and indirect effects of CHT-association on the conformational properties of Aβ peptides. To this end, Aβ peptides in each pH-CHT concentration condition were classified into various groups based on the presence of beta-sheet secondary structure, and whether they were in direct contact with CHT (Fig. 5a illustrates the classification algorithm). Two primary sets: χ, CHT-associated peptides; β, beta-strands, and four subsets: $\beta \cap \chi$, CHT-associated beta-strands; $\beta - \chi$, beta-strands that are not CHT-associated; $\chi - \beta$, CHT-associated peptides that are not beta-strands; $(\beta \cup \chi)^c$, peptides that are neither beta-strands nor associated with CHT, were defined, and end-to-end distances of peptides in each subset were compared. The low populations of alpha-helices prevented statistically meaningful comparisons across such subsets, and thus only beta-strands and random coil peptides were considered in this analysis. Data were gathered from the last 50 ns of two independent replicas, and the population percentages of the subsets are presented as Venn diagrams in Fig. S2.

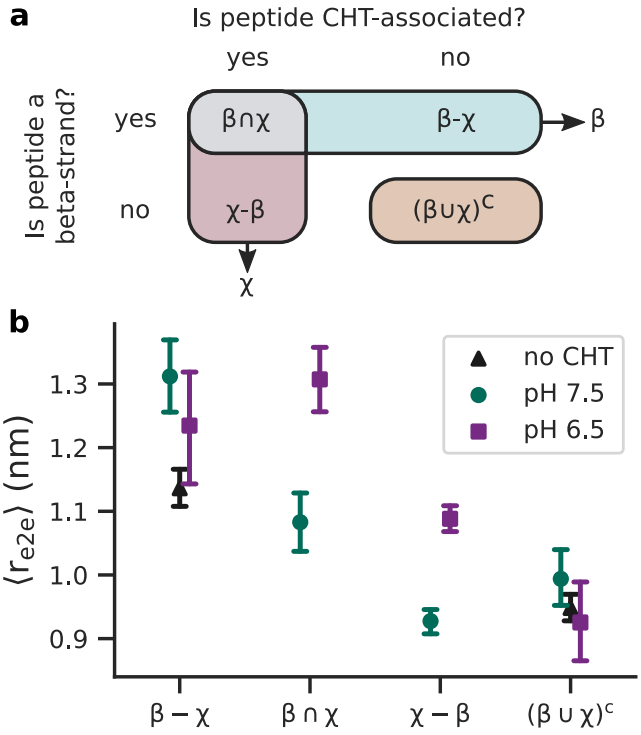

Fig. 5 (a) Algorithm for classification of peptides into sets based on secondary structure and association with CHT. (b) Mean end-to-end distances of peptides of each subset at the 0% CHT control case (black triangles), 1.5% CHT at pH 7.5 (green circles), and 1.5% CHT at pH 6.5 (purple squares).

In Fig. 5b, mean end-to-end distances of peptides in the four subsets are compared for 1.5% CHT at pH 6.5 and pH 7.5, with 0% CHT (no CHT) as reference.

In $(\beta \cup \chi)^c$, mean end-to-end distances ($\langle r_{e2e} \rangle$) are around 0.95 nm for the three samples. While $\langle r_{e2e} \rangle$ was slightly higher at 1.5%

CHT compared to the 0% CHT in $\beta - \chi$, conformations of peptides did not significantly vary between pH 7.5 and 6.5. The same trends were observed at 0.3% CHT (Fig. S2 f). Thus, among peptides that were not in direct contact with CHT, end-to-end distances were largely invariant.

Since nearly all peptides were in direct contact with CHT at 3.0% CHT, sample sizes of $\beta - \chi$ and $(\beta \cup \chi)^c$ were diminishingly small, and statistically not significant (Fig. S2 g, h, i).

On the other hand, peptides in contact with CHT had very different end-to-end distances at pH 6.5 and 7.5. CHT-associated peptides (in $\beta \cap \chi$ and $\chi - \beta$) were consistently more extended at pH 6.5 than at 7.5 in 1.5% CHT (Fig.5b), 0.3% CHT (Fig. S2 f), and 3.0% CHT (Fig. S2 i). Compared to beta-strands not in contact with CHT ($\beta - \chi$), CHT-associated beta-strands ($\beta \cap \chi$) were more extended at pH 6.5, and more collapsed at pH 7.5.

Altogether, these results indicate that the peptide collapsing effect of CHT at pH 7.5, and peptide extending effect of CHT at pH 6.5 requires direct contact with CHT molecules. The conformations of CHT-associated peptides are not inherited by their non-CHT-associated peptide neighbours. A more general inference of these data is that the conformations of Aβ peptides co-assembled with CHT are heterogeneous and depend on their local environments, which in turn are determined by contact with CHT and the pH-dependent degree of cationicity of CHT.

4 Conclusions

We have characterized the mechanistic details of CHT's inhibitory effect on Aβ aggregation using CG-MD simulations. CHT inhibited Aβ aggregation by sequestering peptides, thereby depleting peptide populations in the bulk and limiting multimer growth. The intensity of this sequestration-driven inhibition by CHT was enhanced by its concentration, and pH-dependent degree of cationicity, in agreement with past experimental observations.[10,11]

We also described the ways in which CHT reshaped the conformational landscapes of Aβ peptides. We showed that weakly cationic CHT at pH 7.5 stabilized collapsed peptide conformations, while strongly cationic CHT at pH 6.5 stabilized more extended peptides. Importantly, these conformational changes were largely limited to peptides that were in direct contact with CHT; the inheritance of these conformations from CHT-associated peptides to non-CHT-associated peptide neighbours was weak. This finding of locus-dependent heterogeneity in Aβ conformations offers some insight into why CHT inhibits amyloid aggregation while other polysaccharides, particularly those of the anionic glycosaminoglycan family, strongly induce the formation of ordered amyloid fibrils.[10,35–37] Further studies aimed at delineating the effects of different polysaccharides on amyloid aggregation are planned.

In summary, the mechanistic insights into the fundamental interactions between CHT and Aβ presented in this work could assist in expanding CHT's role in amyloid research, particularly in light of its applications in ECM-mimics for neural cells,[14,15] amyloid detection systems,[13] and anti-amyloid therapeutic nanoparticles and materials.[12,13,16,38]

Data Availability

All files and scripts required to set up and perform the simulations described in this work, along with a brief step-by-step tutorial, can be found at: `https://github.com/suhasgotla/chitosan_amyloid_self-assembly`

Author Contributions

Suhas Gotla: Writing-original draft preparation, Writing-review & editing, Investigation, Visualization, Data analysis. Silvina Matysiak: Conceptualization, Writing-review & editing, Data analysis, Supervision.

Conflicts of interest

There are no conflicts to declare.

Acknowledgements

This research was partially supported by NSF grants CHE-1454948, and CHE-2202281 (S.G. and S.M.), and through computing resources provided by the University of Maryland. S.G. was partially supported by the COMBINE fellowship (NSF DGE-1632976).

Notes and references

1 G.-F. Chen, T.-H. Xu, Y. Yan, Y.-R. Zhou, Y. Jiang, K. Melcher and H. E. Xu, *Acta Pharmacologica Sinica*, 2017, **38**, 1205–1235.
2 M. Ahmed, J. Davis, D. Aucoin, T. Sato, S. Ahuja, S. Aimoto, J. I. Elliott, W. E. Van Nostrand and S. O. Smith, *Nature Structural & Molecular Biology*, 2010, **17**, 561–567.
3 D. J. Selkoe and J. Hardy, *EMBO Molecular Medicine*, 2016, **8**, 595–608.
4 E. N. Cline, M. A. Bicca, K. L. Viola and W. L. Klein, *Journal of Alzheimer's Disease*, 2018, **64**, S567–S610.
5 J. Fantini, H. Chahinian and N. Yahi, *Protein Science*, 2020, **29**, 1748–1759.
6 M. Shi, F. Chu, F. Zhu and J. Zhu, *Frontiers in Aging Neuroscience*, 2022, **14**, year.
7 M. Tolar, S. Abushakra and M. Sabbagh, *Alzheimer's & Dementia*, 2020, **16**, 1553–1560.
8 C. A. Lemere, *Molecular Neurodegeneration*, 2013, **8**, 36.
9 C. M. T. Parrocha and J. S. Nowick, *Peptide Science*, 2022, **n/a**, e24289.
10 J. J. Valle-Delgado, M. Alfonso-Prieto, N. S. de Groot, S. Ventura, J. Samitier, C. Rovira and X. Fernàndez-Busquets, *The FASEB Journal*, 2010, **24**, 4250–4261.
11 H. Liu, B. Ojha, C. Morris, M. Jiang, E. P. Wojcikiewicz, P. P. N. Rao and D. Du, *Biomacromolecules*, 2015, **16**, 2363–2373.
12 A. Jha, V. Ghormade, H. Kolge and K. M. Paknikar, *Journal of Materials Chemistry B*, 2019, **7**, 3362–3373.
13 W. Wang, M. Liu, W. Gao, Y. Sun and X. Dong, *ACS Applied Materials & Interfaces*, 2021, **13**, 55879–55889.
14 R. J. Miller, C. Y. Chan, A. Rastogi, A. M. Grant, C. M. White, N. Bette, N. J. Schaub and J. M. Corey, *Journal of Biomaterials Science, Polymer Edition*, 2018, **29**, 1625–1642.

15 N. L. Francis, P. M. Hunger, A. E. Donius, B. W. Riblett, A. Zavaliangos, U. G. K. Wegst and M. A. Wheatley, *Journal of Biomedical Materials Research Part A*, 2013, **101**, 3493–3503.

16 L. Zhu, R. Li, S. Jiao, J. Wei, Y. Yan, Z. A. Wang, J. Li and Y. Du, *Marine Drugs*, 2020, **18**, 488.

17 Z. Songjiang and W. Lixiang, *AAPS PharmSciTech*, 2009, **10**, 900.

18 S. Roy Chowdhury, S. Mondal, B. Muthuraj, S. N. Balaji, V. Trivedi and P. Krishnan Iyer, *ACS Omega*, 2018, **3**, 8059–8066.

19 X. Dai, W. Hou, Y. Sun, Z. Gao, S. Zhu and Z. Jiang, *International Journal of Molecular Sciences*, 2015, **16**, 10526–10536.

20 S. Jia, Z. Lu, Z. Gao, J. An, X. Wu, X. Li, X. Dai, Q. Zheng and Y. Sun, *International Journal of Biological Macromolecules*, 2016, **83**, 416–425.

21 S. J. Marrink, H. J. Risselada, S. Yefimov, D. P. Tieleman and A. H. de Vries, *The Journal of Physical Chemistry B*, 2007, **111**, 7812–7824.

22 H. Xu and S. Matysiak, *Chemical Communications*, 2017, **53**, 7373–7376.

23 S. Gotla, C. Tong and S. Matysiak, *ACS Applied Nano Materials*, 2022, **5**, 6463–6473.

24 A. Sahoo, H. Xu and S. Matysiak, *Physical Chemistry Chemical Physics*, 2019, **21**, 8559–8568.

25 A. Sahoo and S. Matysiak, *Physical Chemistry Chemical Physics*, 2021, **23**, 20627–20633.

26 D. H. de Jong, G. Singh, W. F. D. Bennett, C. Arnarez, T. A. Wassenaar, L. V. Schäfer, X. Periole, D. P. Tieleman and S. J. Marrink, *Journal of Chemical Theory and Computation*, 2013, **9**, 687–697.

27 S. J. Ganesan and S. Matysiak, *Journal of Chemical Theory and Computation*, 2014, **10**, 2569–2576.

28 S. J. Ganesan, H. Xu and S. Matysiak, *Physical Chemistry Chemical Physics*, 2016, **18**, 17836–17850.

29 S. O. Yesylevskyy, L. V. Schäfer, D. Sengupta and S. J. Marrink, *PLOS Computational Biology*, 2010, **6**, e1000810.

30 D. J. Evans and B. L. Holian, *The Journal of Chemical Physics*, 1985, **83**, 4069–4074.

31 M. Parrinello and A. Rahman, *Journal of Applied Physics*, 1981, **52**, 7182–7190.

32 T. Darden, D. York and L. Pedersen, *The Journal of Chemical Physics*, 1993, **98**, 10089–10092.

33 B. Hess, H. Bekker, H. J. C. Berendsen and J. G. E. M. Fraaije, *Journal of Computational Chemistry*, 1997, **18**, 1463–1472.

34 S. Pronk, S. Páll, R. Schulz, P. Larsson, P. Bjelkmar, R. Apostolov, M. R. Shirts, J. C. Smith, P. M. Kasson, D. van der Spoel, B. Hess and E. Lindahl, *Bioinformatics*, 2013, **29**, 845–854.

35 R. Bravo, M. Arimon, J. J. Valle-Delgado, R. García, N. Durany, S. Castel, M. Cruz, S. Ventura and X. Fernàndez-Busquets, *Journal of Biological Chemistry*, 2008, **283**, 32471–32483.

36 B. Khurshid, A. U. Rehman, R. Luo, A. Khan, A. Wadood and J. Anwar, *ACS Omega*, 2022, **7**, 15132–15144.

37 M. Islam, E. Argueta, E. P. Wojcikiewicz and D. Du, *ACS Chemical Neuroscience*, 2022, **13**, 3034–3043.

38 Z. Jiang, X. Dong and Y. Sun, *Carbohydrate Research*, 2018, **461**, 11–18.